ELSEVIER

0308-0161(95)00091-7

Int. J. Pres. Ves. & Piping 66 (1996) 141–153

0308–0161/96/$15.00

RECOVERY OF CREEP PROPERTIES OF THE NICKEL-BASE SUPERALLOY NIMONIC 105

R. B. Girdwood* **and R. W. Evans+**

*Division of Materials Science and Technology, CSIR, P O Box 395, Pretoria, 0001, Republic of South Africa
+Department of Materials Engineering, University College, Singleton Park, Swansea, SA2 8PP, United Kingdom

ABSTRACT

Uniaxial constant stress creep tests were performed on the wrought nickel-base superalloy Nimonic 105. Entire creep curves were recorded and curve shapes analysed using the θ Projection Concept. Rejuventive procedures were applied to pre-crept samples and creep recovery quantitatively assessed.

Microstructural damage occurring during the creep of Nimonic 105 was studied. Creep strength is lost by the coarsening of the γ' precipitate and grain boundary carbides.

The θ Projection Concept relates damage to strain using a Kachanov model. Damage accumulation can be measured and any rejuvenation procedure can be assessed for effectiveness by curve shape analysis.

It is found that complete re-solution heat treatment is able to recover the microstructure and, on re-testing, significant creep curve recovery is observed. An additional heat treatment was performed under hydrostatic pressure of 100MPa in argon to remove cavities. Complete recovery of the creep curve was achieved even when this procedure was applied late in the tertiary stage of creep.

KEYWORDS

creep; Theta Projection Concept; recovery of creep properties; rejuvenation; nickel-base superalloys; Nimonic 105.

INTRODUCTION

The most common application for nickel-base superalloys is as turbine blades in aircraft gas-turbine engines. Turbine blades are subject to a complex combination of stresses: hot gas temperatures of ≈ 1700K, outside-to-inside temperature gradients of ≈150Kmm^{-1} in well cooled blades and centrifugal accelerations of about 200 000g. Thus, aerodynamic excitation of the natural frequency of vibration can lead to high cycle fatigue. Alternating mechanical and thermal stresses during take-off and landing cycles can lead to low cycle fatigue. Creep mechanisms are activated during steady state operation. In general, structural changes occur under the effects of temperature, time and stress with the result that components are subject to continual degradation of their properties, particularly their creep strength.

In order to quantify creep damage recovery a baseline from which to measure damage accumulation is required. Conventionally, normal creep curves are described as consisting of three stages: a primary stage during which creep deformation decelerates, a secondary stage with constant creep rate, and a tertiary stage during which deformation accelerates until final failure. Creep curves are

characterised by three parameters, steady state creep rate, $\dot{\varepsilon}_s$, time to failure, t_f, and the strain to failure, ε_f. The development of constitutive equations has been limited to the secondary stage and it is generally accepted that $\dot{\varepsilon}_s$ can be related to stress, σ, and temperature, T, by a power law:

$$\dot{\varepsilon}_s = A\sigma^n \exp\left(-\frac{Q_c}{RT}\right), \tag{1}$$

where, A is a material constant, R is the universal gas constant and Q_C is the activation energy for creep. Variations of the values of n and Q_C with stress and temperature have been taken as evidence for different creep mechanisms. Extrapolation of rupture time, t_f, has been based on time-temperature parametric methods. The traditional description of creep behaviour by the three parameters of $\dot{\varepsilon}_s$, t_f and ε_f is not only unable to provide long term strain data required by modern computer-based design procedures, they do not provide any data relating to the degradation of the material under consideration.

It is therefore highly desirable to use new methods which, based on relatively short term experiments, will predict long term creep curves from which any creep parameter can be derived. One such method, the θ Projection Concept[1], has been proved successful for many engineering materials[1]. The benefits of whole creep curve analysis are many-fold. Any creep property can be derived from creep curves predicted by a single equation. Since creep damage is usually manifest by an accelerating tertiary curve, rejuvenative procedures can be quantitatively assessed by comparison to an accurately predicted baseline.

In this study, high precision constant stress creep tests have been undertaken on Nimonic 105. The creep curves obtained are used as a database from which predictions of creep properties are made by using the θ Projection Concept approach to creep modelling. Rejuvenative procedures are applied and the resultant creep curves are compared to the θ predicted curve and quantitative measurements of damage recovery are achieved. Constant stress tests are justified for rejuvenation testing as microstructural investigations showed there to be no, or very little, loss in load bearing area as a result of internal damage.

THE θ PROJECTION CONCEPT

The θ Projection Concept, in its most general form, describes the variation of creep strain, ε, with time, t, in the following manner:

$$\varepsilon = \theta_1(1-e^{-\theta_2 t}) + \theta_3(1+\omega_o)(e^{\theta_4 t}-1) + \varepsilon_o \tag{2}$$

where ε_o is the initial state of strain and ω_o is the initial state of damage.

In general both ε_o and ω_o = 0 so that eqn (2) reduces to the more common form:

$$\varepsilon = \theta_1(1-e^{-\theta_2 t}) + \theta_3(e^{\theta_4 t}-1). \tag{3}$$

In attempts to determine relationships between the θ_i and stress and temperature it has been reported by Evans et al that, for $1/2Cr1/2Mo1/4V$ steel[1], sintered MgO[2] and other materials[1,3-7]

analysed in this manner, at each creep temperature studied, a linear relationship exists between ln θ_i and stress. Furthermore, since only narrow ranges of temperature are usually studied the θ data at any stress can also be represented by linear plots of $\log \theta_i$ against temperature. Thus, each θ parameter can be conveniently described by a general empirical function of stress and temperature as

$$\log \theta_i = a_i + b_i\sigma + c_iT + d_i\sigma T \qquad (4)$$

where a_i, b_i, c_i and d_i are constants for the material (i = 1 to 4).
The coefficients are evaluated by multi-linear least squares regression analysis of the test data. Once the a_i, b_i, c_i and d_i are known, the material is characterised for the temperature range examined and accurate long term predictions can be made for lower stresses.

RESULTS

θ representation

A series of high precision, constant stress creep tests undertaken over the temperature range 1098K-1198K yielded θ parameters varying according to eqn(4) with constants displayed in table 1.

Table 1 Stress and temperature dependence of the θ_i.

	a_i	b_i	c_i	d_i
ln θ_1	1.44314	-1.65065×10^{-2}	-5.46750×10^{-3}	1.28904×10^{-5}
ln θ_2	-53.1418	1.91667×10^{-2}	3.33088×10^{-2}	7.15851×10^{-7}
ln θ_3	0.34284	-1.06482×10^{-2}	-6.63331×10^{-3}	1.58298×10^{-5}
ln θ_4	-41.2686	-1.29435×10^{-1}	2.09343×10^{-2}	1.33974×10^{-4}

Plots of the $\ln\theta_i$ vs stress are linear. Consequently, it is possible to calculate entire creep curves and all creep properties at any stress and temperature using eqn(3) with the constants in table 1. This model has no failure criterion.

A failure criterion which assumes a linear variation of ln ε_f with stress, σ, and temperature, T, in the same fashion as the ln θ_i is found to characterise the strain to failure, ε_f, well

$$\ln \varepsilon_f = x_1 + x_2\sigma + x_3T + x_4\sigma T \qquad (5)$$

with the x_i displayed in table 2.

Table 2 Stress and temperature dependence of failure strain, ε_f.

	x_1	x_2	x_3	x_4
ln ε_f	-8.50182	3.87152×10^{-2}	5.23133×10^{-3}	-3.60991×10^{-5}

Now that a baseline from which to measure any rejuvenative procedures that may "heal" damage is in place it is important to identify the "damage" modes and construct rejuvenative procedures.

MICROSTRUCTURAL OBSERVATIONS

In order to determine what rejuvenative procedures will "heal" damage it is necessary to determine what microstructural factors contribute to the accumulation of damage, ω.
The literature generally reports degradation of γ' and grain boundary carbides and the development of grain boundary cavities to be the main creep life consuming factors. Thus, crept specimens are examined to determine how these factors vary within the testing regime.

Figure 1(a) shows the carbide morphology in the as heat treated state. As anticipated, the carbides are of the $M_{23}C_6$ type and are concentrated at the grain boundaries as discrete particles. The carbides are encased in a thin envelope of γ'. Figure 1(b) shows the γ' particles in the as heat treated state. They are evenly distributed throughout the grains and occur as spheres, and to a lesser extent as cubes, with a mean diameter of approximately 85nm.

Figures 2(a) and 2(b) show typical structures after creep testing to failure at 1148K and a stress of 170MPa. The micro graphs are presented for structures in the gauge length and in the grip section of the specimen so that crept and uncrept microstructures may be compared.

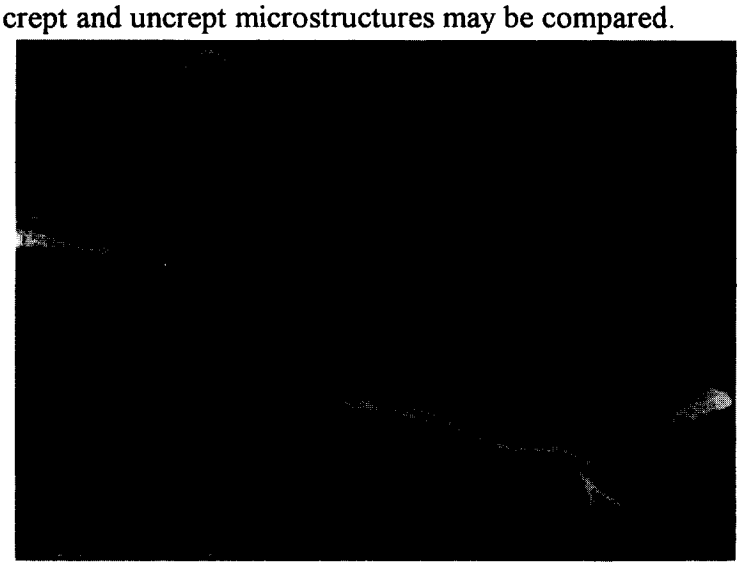

Fig. 1(a). Grain boundary carbide morphology in the as heat treated state.

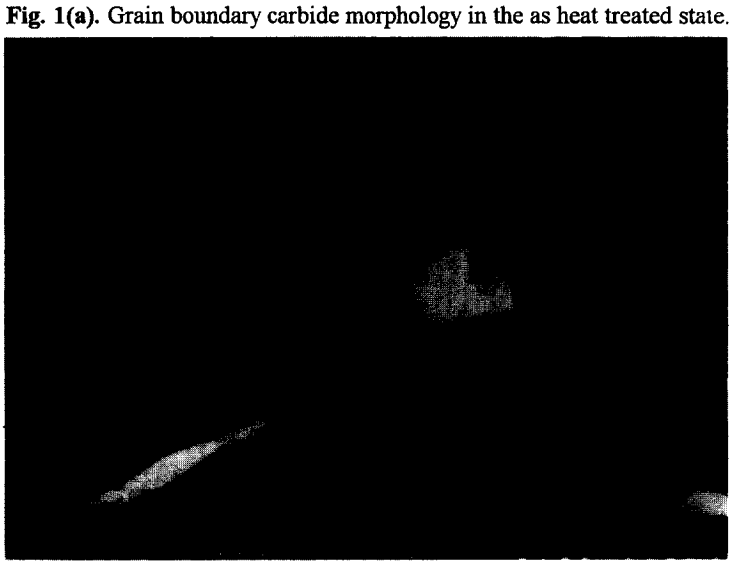

Fig. 1(b). γ' morphology in the as heat treated state.

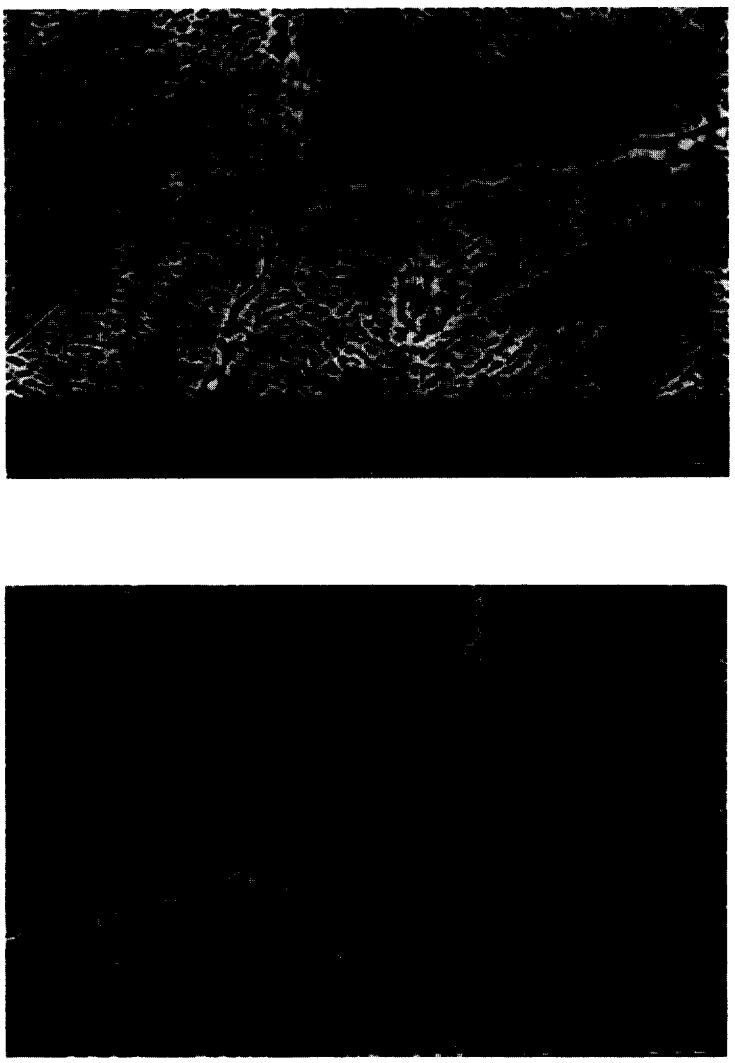

Fig. 2(b) γ' and carbide morphology in the uncrept section of the specimen crept to fracture at 170MPa and 1148K. Only ageing is apparent and the general extent of the damage is less than in fig. 1(a).

It is clearly observed from the micro graphs that at any temperature as the stress decreases and time at temperature increases the γ' coarsens. When comparing the crept and uncrept sections it is also observed that in tests of longer duration (lower stress), even though γ' coarsening occurs, the γ' elongates in the crept sections whilst maintaining its spherical shape in the uncrept regions. As the temperature rises these effects are exaggerated. Similarly, as stress decreases and test duration increases at any one temperature, the γ' coarsen and elongate, the grain boundaries become thicker with γ' and the carbides break up and coarsen. In the grip section, where no creep occurs, the γ' coarsens but remains spherical whilst the grain boundaries and carbides remain relatively unaffected.

Optically resolvable cavitation in the region of the fracture was observed. Although assumed to be present, cavitation was not resolvable in regions far away from the fracture and was not detected in any interrupted testing. There is a clear trend showing that at all temperatures greatest cavity density occurs at lowest stress. It was not possible to determine a threshold stress below which cavitation is dominant and above which triple point cracking is dominant. Throughout the range of stress and

temperature, cavitation is dominant but triple point cracks are always present in small quantities. All cavitation is intergranular in nature.

Discussion

The literature reports that the creep strength of nickel based superalloys is derived from a complex interaction between solid solution strengthening mechanisms, precipitate hardening and grain boundary carbides. Since the purpose of this work is to ascertain what damage occurs during the creep of Nimonic 105 and not the detailed mechanisms by which it happens, some simple observations will be made without attempting a detailed description of the mechanisms of tertiary creep of Nimonic 105. The aim of microstructural observation is to determine what procedures may be appropriate for the rejuvenation of the creep properties of Nimonic 105.

The general microstructural observations show that there is a clear change in the morphology of the γ' with time and temperature (Ostwald ripening). The γ' elongation is more pronounced in the longer tests. The γ' envelope in the grain boundaries thickens with time and the carbides coarsen. In the uncrept regions of the creep specimen the γ' simply overages whilst the grain boundaries and the carbides remain relatively unchanged. These are the most apparent manifestations of damage and therefore in order to repair this damage it is necessary to return the γ' and the grain boundary carbides to their original state. Cavitation, although not apparent in the interrupted tests, is reported in the literature as being detectable by accurate density measurements therefore any rejuvenative procedure must attempt to heal small cavities.

The heat treatment applied to the virgin material is a three stage heat treatment: solution treatment at 1423K takes all γ' and most of the carbides into solution, and on cooling, very fine γ' precipitates. On ageing at 1323K, some or all of the γ' re dissolves, further ageing at 1123K gives spherical γ' particles. This heat treatment points to a possible rejuvenative procedure.

REJUVENATIVE PROCEDURES

Three methods have been used in an attempt to recover creep properties of Nimonic 105. All methods are based on the initial heat treatment regime applied to the virgin material. The procedures are as follows:

1. High temperature anneal (16hrs at 1323K). This treatment dissolves the γ' phase but not the carbides. A standard ageing treatment (16hrs at 1123K) is employed to regain the original γ' distribution. This procedure is chosen to indicate the effect of overageing on creep properties.
2. Complete commercial re-solution heat treatment as detailed above. This procedure recreates the γ' size and distribution and takes the carbides back into solution before re precipitating them back on the grain boundaries. Grain growth is possible. This treatment is chosen to indicate the effect of grain boundary carbides on creep properties.
3. Hot isostatic pressing (HIP) for 4hrs at 1323K and 105MPa in Argon followed by the commercial re solution heat treatment to recover the original microstructure. This procedure is chosen to indicate the effect of grain boundary cavitation on creep properties by attempting to sinter non- surface connected non- oxidised cavities.

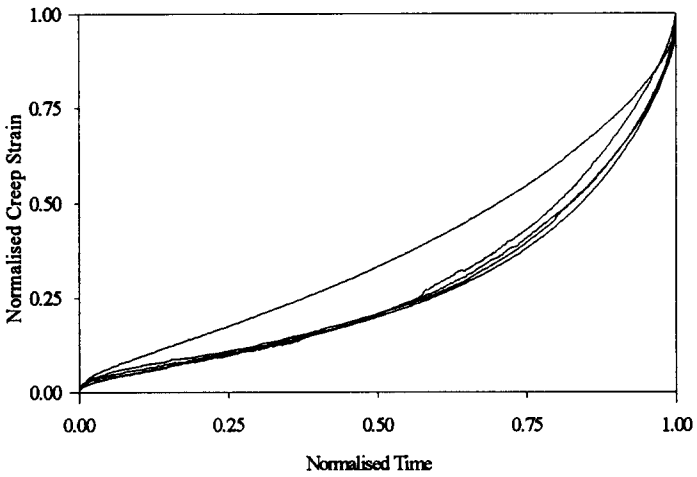

Fig. 3 Normalised creep curves to show the variation of creep curve shape over the entire range of creep stress and temperature.

Figure 3 shows that the creep curves of Nimonic 105 are essentially tertiary in nature and that there is no change in creep curve shape over the range of testing conditions applied in this study. This indicates that the damage mechanisms are the same throughout the testing regime. This is very convenient since rejuvenative procedures need only be applied at one stress and temperature in order to assess their success over the entire range of testing conditions. To this end, the intermediate temperature, 1148K, is chosen to study rejuvenative procedures. A stress of 170MPa is chosen to give a test lasting about 500hrs.

In order to assess the effect of the rejuvenative procedures on the severity of damage, creep tests were interrupted at $4\dot{\varepsilon}_m$, $8\dot{\varepsilon}_m$ and $16\dot{\varepsilon}_m$. These points are early, mid- and late tertiary. The reasons behind these choices are indicated by the microstructural observations:

- During the early stages of tertiary creep ($4\dot{\varepsilon}_m$), damage is limited to overageing and some elongation of the γ' precipitate. Little damage to carbides or appreciable cavitation are observed.
- During the mid stages of tertiary creep ($8\dot{\varepsilon}_m$), γ' ageing and elongation are more pronounced. Carbide and grain boundary damage become more pronounced. Cavitiation may begin but none is evident in any of the observations made.
- During the late stages of tertiary creep ($16\dot{\varepsilon}_m$), severe γ', carbide and grain boundary damage occurs. Cavitiation, although not observed is reported in the literature to be present.

High temperature anneal

Figure 4 shows the microstructural state of a specimen crept to $8\dot{\varepsilon}_m$,annealed and aged. The γ' has not returned to its original state (fig. 1(b)). Although there is fine γ' present it is sparse, large precipitates have grown at the expense of smaller ones. The grain boundary carbides show little change from the virgin state.

Fig. 4 γ' and carbide morphology after creep to $8\dot{\varepsilon}_m$ and then given the high temperature anneal (16hrs 1323K, AC, 16hrs 1123K, AC).

Examination, after failure, of the crept section of the specimen crept to $8\dot{\varepsilon}_m$ showed the γ' particles to be very small and elongated. Grain boundary carbides were extremely sparse and the grain boundaries were badly damaged.

Complete re-solution heat treatment

Figure 5 shows the microstructural state of a specimen crept to $8\dot{\varepsilon}_m$ and then given the complete re-solution heat treatment. The γ' and $M_{23}C_6$ carbide morphology and distribution have been fully recovered. Compare with virgin heat treatment in figs. 1(a) and (b).

Examination, after failure, of the crept section of the specimens pre-crept to $4\dot{\varepsilon}_m$ and $8\dot{\varepsilon}_m$ respectively showed that γ' had elongated and coarsened. The grain boundaries were thick with γ'. Carbides had broken up.

Fig. 5 γ' and carbide morphologies after creep to $8\dot{\varepsilon}_m$ and then given the complete resolution heat treatment (4hrs 1423K, AC, 16hrs 1323K, AC, 16hrs 1123K, AC)

HIP and complete re-solution heat treatment

Figure 6 show the microstructure after the HIP and heat treatment have been applied to specimens crept to $16\dot{\varepsilon}_m$ and failure respectively. Figure 6 shows that γ' and carbide morphology and distributions are fully recovered (compare with fig. 1(a)).

Examination, after failure, of the specimens precrept to $4\dot{\varepsilon}_m$, $8\dot{\varepsilon}_m$ and $16\dot{\varepsilon}_m$ respectively showed γ' damage to be limited to slight coarsening and elongation for the specimen precrept to $4\dot{\varepsilon}_m$. Grain boundaries and carbides appear relatively unaffected. Damage appears similar to that in the untreated specimen in fig. 1(a). As the creep rate increases to $8\dot{\varepsilon}_m$ and $16\dot{\varepsilon}_m$ before interruption for rejuvenation, γ' shows increasing coarsening and elongation. The most marked effect is in the thickening of the grain boundaries and break up of the carbides. Cavitation and gross carbide degeneration are apparent.

Fig. 6 γ' and carbide morphology after creep to $16\dot{\varepsilon}_m$, HIPed (4hrs 1323K 100MPa in Argon) and fully re-solution heat treated.

Discussion on rejuvenative processes

Creep tests and microstructural studies have been undertaken at 170MPa 1148K for three different heat treatments applied after creep to $4\dot{\varepsilon}_m$, $8\dot{\varepsilon}_m$ and $16\dot{\varepsilon}_m$ in an attempt to rejuvenate creep properties of Nimonic 105. A preliminary assessment of damage recovery can be made on the basis of the traditional measures of creep performance (minimum creep rate, time to failure and ductility). Comparison of these quantities with the 95% confidence intervals of the sample lead to the following general observations:

- minimum creep rate is recovered in all cases.
- time to failure is not recovered by annealing at 1323K for 16hrs followed by ageing at 1123K for 16hrs,
- ductility is only fully recovered when HIP is combined with the complete re-solution heat treatment after creep to late tertiary.

Due to the large scatter in the creep properties of the sample, minimum creep rate, time to failure and ductility are not suitable references for quantifying creep damage recovery. Instead, it may be appropriate to assess the recovery of creep curve shape using the θ Projection Concept.

The θ Projection Concept utilises the Kachanov model[8] to give the relationship between creep strain and damage as:

$$\frac{d\varepsilon_t}{dt} = \frac{\beta}{\alpha}(1+\omega) \tag{6}$$

$$\frac{d\omega}{dt} = C\frac{d\varepsilon_t}{dt} \tag{7}$$

where ε_t is tertiary strain, β/α is the steady state creep rate of undamageable material and C is a constant.

Eqn (6) illustrates that ω is simply the percentage deviation of the creep curve of a damageable material from that of an undamageable one. Similarly, since these relationships are known for Nimonic 105, the damage evolution for a rejuvenated curve can be measured relative to that of a curve derived from the standard θ formulation, eqn (3). The damage evolution of the rejuvenated curve is obtained by making the following substitutions:

$$\dot{\varepsilon}_\theta = \frac{\beta}{\alpha} \qquad \text{and} \qquad \dot{\varepsilon}_{rej} = \frac{d\varepsilon_t}{dt}$$

where $\dot{\varepsilon}_\theta$ is the θ predicted minimum creep rate of an unrejuvenated specimen and $\dot{\varepsilon}_{rej}$ is the creep rate of a rejuvenated specimen.

So that,

$$\omega_{rej} = \frac{\dot{\varepsilon}_{rej}}{\dot{\varepsilon}_\theta} - 1 \tag{8}$$

where ω_{rej} is the damage evolution of a rejuvenated specimen relative to a θ predicted curve.

If $\omega_{rej} = 0$ at the beginning of tertiary creep then $\omega_o = 0$ in eqn (2), otherwise ω_o has a finite value given by eqn (8). Plotting ω_{rej} against ε_t then provides a means of quantitatively assessing the success of rejuvenative procedures.

Figures 7-9 rationalise creep damage, ω, for each interruption by plotting ω (from eqn (8)) against creep strain. Figures 7-9 illustrate ω evolution for the creep specimens given each of the three rejuvenation treatments after creep to $4\dot{\varepsilon}_m$ and $8\dot{\varepsilon}_m$ respectively. Figure 9 shows the same information for the test interrupted after creep to $16\dot{\varepsilon}_m$ before being HIPed and re-solution heat treated. Negative damage in these figures has no meaning, they are as a result of the method of calculating ω.

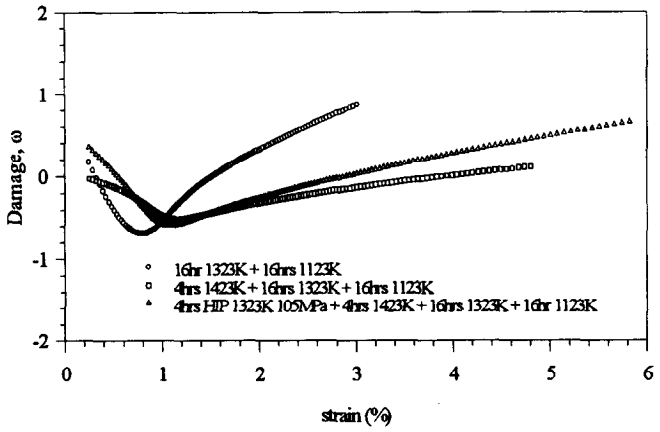

Fig. 7 Plot of damage, ω, measured relative to the θ curve for creep at 1148K, 170MPa vs creep strain for each rejuvenation. Curves are for each rejuvenation applied after creep to $4\dot{\varepsilon}_{min}$.

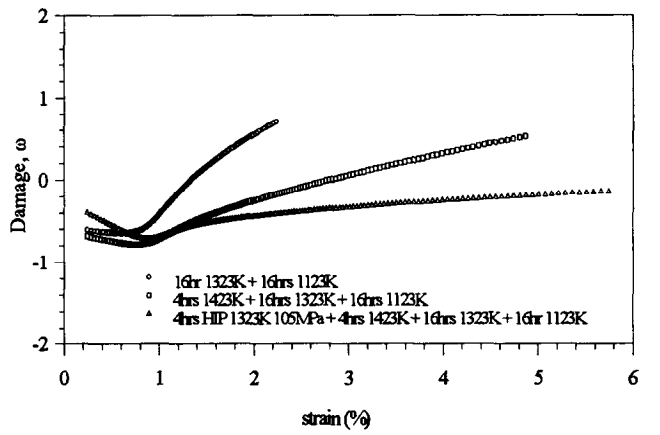

Fig. 8 Plot of damage, ω, measured relative to the θ curve for creep at 1148K, 170MPa vs creep strain for each rejuvenation. Curves are for each rejuvenation applied after creep to $8\dot{\varepsilon}_{min}$

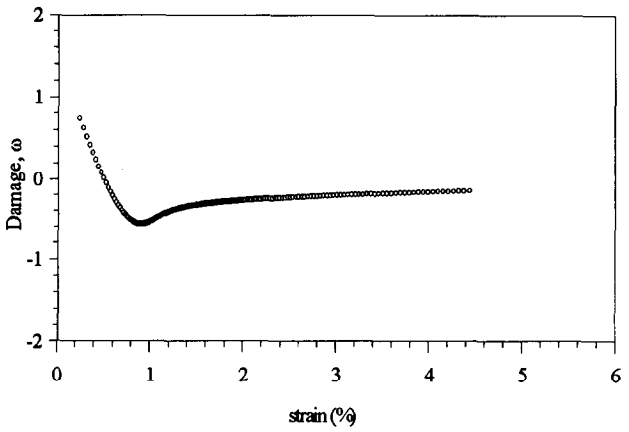

Fig. 9 Plot of damage, ω, measured relative to the θ curve for creep at 1148K, 170MPa vs creep strain for HIP followed by complete resolution heat treatment. Curve is for the rejuvenation applied after creep to $16\dot{\varepsilon}_{min}$.

The figures clearly show that no matter when applied, the high temperature anneal causes rapid acceleration of ω (with respect to ε). Ductility is severely reduced in the rejuvenated specimen. The purpose of the high temperature anneal was to determine the effect of γ' recovery. Microstructural observation showed that γ' was not recovered, in fact, it was adversely affected by the heat treatment.

Specimens crept to early ($4\dot{\varepsilon}_m$) and mid- ($8\dot{\varepsilon}_m$) tertiary before receiving complete re-solution heat treatment show a much reduced dω/dε. There is little difference in dω/dε for the specimens interrupted at 4- and $8\dot{\varepsilon}_m$ before rejuvenation. A slight reduction in ductility is observed. This treatment was to determine the effect of recovering both γ' and carbide morphologies. Microstructural studies showed that original microstructures were recovered. Since $d\omega/d\varepsilon \neq 0$ in figs. 7 and 8, full recovery is not achieved.

Specimens crept to early ($4\dot{\varepsilon}_m$) and mid- ($8\dot{\varepsilon}_m$) and late ($16\dot{\varepsilon}_m$) tertiary before receiving HIP and re-solution heat treatment show a decrease in dω/dε as interruption creep rate is increased (figs. 7-9). When interrupted at early tertiary there is little difference in $d\omega/d\varepsilon$ between specimens re-solution heat treated and those HIPed and re-solution heat treated (fig. 7). This indicates that HIP has no effect on the recovery of creep properties at this stage. However, dω/dε after treatment at mid tertiary is lower for the HIPed specimen than for the unHIPed one indicating that HIP is eliminating damage that the re-solution heat treatment cannot. When applied at late tertiary, HIP results in the full recovery of creep properties (dω/dε is very small).

CONCLUSIONS

Conventionally, the effectiveness of rejuvenative procedures have been assessed with respect to recovery of minimum creep rates and strain and time to failure. The basic creep design procedures such as the Larson-Miller parameter, life trend diagrams, Monkman-Grant relationship and other

parametric methods, usually used for prediction purposes rely on an accurate and reproducible knowledge of these traditional measures of creep. It is well known that the scatter bands encountered in measuring these quantities yields unacceptable uncertainty. Hence, when assessing rejuvenative procedures it may happen that time to failure measured on a specimen subject to rejuvenative heat treatments may be on the opposite end of the scatter band to that measured on a reference specimen. Clearly, when the rejuvenated quantity is on the lower end of the scatter band and the reference test on the upper end of the scatter band a false impression of the effectiveness of the rejuvenative procedure is formed. The obvious way of overcoming this is to do a large number of tests so that a statistically meaningful measure of these quantities can be achieved. In practise this means large costs and long testing programmes which are clearly undesirable.

On the other hand, the creep curve shape shows reduced statistical variation and conveys more information with regard to dominant creep processes. Surely then, rejuvenative procedures can be better measured by observing parameters which define the creep curve shape rather than by arbitrarily chosen variables which often bear no significance to the creep processes that are active.

The θ Projection Concept has been used in this study and has shown that with relatively few short term tests a very good and consistent measure of the effectiveness of rejuvenative procedures can be achieved. The θ Projection Concept is formed on the basis that creep consists of the two competing processes: decaying creep rate associated with deformation processes governing primary creep and acceleration in creep rate due to tertiary processes, which can be considered as "damaging" processes. The minimum creep rate is achieved when these two processes are in balance. The θ equations can be derived using initial conditions of damage and strain and the damage evolution can be characterised.

The relationship between creep strain and damage indicates that damage is strain controlled, therefore, plotting the damage variable against strain for different rejuvenative procedures gives a good measure of the effectiveness of the procedure. This is clearly apparent in figs. 7-9.

The tests used in this work were purely tensile in nature. There is nothing to say that this approach will give good results when the stress state is multi-directional. Indeed, the indications are that damage is not scalar but a vector and when used in a multi-axial state of stress, the damage variable will have to be formulated as a tensor. However, this preliminary work provides a good indication of the effectiveness of rejuvenative procedures by observing the tensile case.

REFERENCES

1. R. W. Evans and B. Wilshire, "Creep of Metals and Alloys", Institute of Metals, London, 1985
2. R. W. Evans, P. J. Scharnning and B. Wilshire, "Creep Behaviour of Crystalline Solids", Pineridge Press, Swansea, 1985, p201
3. R. W. Evans, T. Murakami and B. Wilshire, *Br. Ceram. Trans. J.*, **2** (1988) 54
4. S. G. R. Brown, R. W. Evans and B. Wilshire, *Mat. Sci. Engng.*, **84** (1986) 147
5. R. W. Evans and B. Wilshire, *Mat. Sci. Tech.*, **3** (1987) 701
6. S. G. R. Brown, R. W. Evans and B. Wilshire, *Mat. Sci. Tech.*, **3** (1987) 23
7. I. Beden, S. G. R. Brown, R. W. Evans and B. Wilshire, *Res. Mechanica*, **22** (1987) 45
8. R. W. Evans, "VIII Int. Symp. on Creep Resistant Metallic Materials", Creep Czechoslovakia, Zhlin, 1991, p20